Supplementary Information

Synergy between Structural Rigidity and Cluster Defects in Bright Near-Infrared Cr^{3+}-based Phosphor for Excellent Thermal Stability and Long Afterglow

Annu Balhara,[1,2] Santosh K. Gupta,[1,2*] Brindaban Modak,[2,5] Malini Abraham,[3,4] Ashok Kumar Yadav[6], Harshini V. Annadata,[6] Subrata Das,[3,4] Narender Singh Rawat,[2,7] Kathi Sudarshan[1,2]

[1]Radiochemistry Division, Bhabha Atomic Research Centre, Trombay, Mumbai-400085, India

[2]Homi Bhabha National Institute, Anushaktinagar, Mumbai – 400094, India

[3]Materials Science and Technology Division, CSIR-National Institute for Interdisciplinary Science and Technology, Thiruvananthapuram, Kerala 695019

[4]Academy of Scientific and Innovative Research (AcSIR), Ghaziabad-201002, India

[5]Chemistry Division, Bhabha Atomic Research Centre, Trombay, Mumbai-400085, India

[6]Beamline Development & Application Section, Bhabha Atomic Research Centre, Mumbai 400085

[7]Radiological Physics and Advisory Division, Bhabha Atomic Research Centre, Trombay, Mumbai-400085, India

****To whom correspondence should be addressed. Electronic mail: *santoshg@barc.gov.in/ santufrnd@gmail.com (SKG)***

S1. Instrumentation

The powder XRD patterns were acquired on a Proto-AXRD bench top system in the 2θ range of 15-80° and a scan rate of 1°/min. Fourier Transform Infrared Spectroscopy (FTIR) was performed with a diamond ATR mode on a Bruker Alpha FTIR spectrometer in the scanning range from 400 to 4000 cm^{-1}. The scanning electron microscopy (SEM) and energy dispersive spectroscopy (EDS) were performed on a SEM (Model: JEOL ICM6000Plus-7E, Japan) system. Transmission electron microscopy (TEM) measurements were done on a JEOL, JEM-2100 TEM microscope with an operating voltage of 200 kV. The XPS measurements were carried out on a SPECS instrument with a PHOBIOS 100/150 delay line detector (DLD). The PL and PLE spectra were recorded with a continuous Xenon lamp (450

W) source on a FLS-1000 fluorescence spectrometer (Edinburgh Instruments, U.K.), and visible-PMT as the detector. Emission photographs were captured under 365 nm UV lamp by a Nikon camera. Low temperature dependence PL studies were performed using cryostat assembly with FLS-1000 fluorescence spectrometer and liquid nitrogen as coolant. Temperature dependent spectra and power dependent spectra was measured using an Ocean optics spectrophotometer that has a Maya 2000 PRO with a 420 nm LEDs as excitation source. Quantum yield measurements were carried out using integrated sphere. Thermoluminescence measurements were carried out on Riso TL/OSL-DA-15 reader system equipped with a 7.5 mm Hoya U-340 detection filter. Low-temperature electron paramagnetic resonance (EPR) studies at 100 K were performed on a Bruker EMX Series spectrometer using X band frequency (9.5 GHz) and 100 kHz field modulation. The Cu X-ray tube was operated at 40kV and 30 mA to irradiate the sample for 60 seconds and then the decay of intensity with time was measured after switching off the X-rays.

S2. EXAFS Analysis

An X-ray Absorption Spectroscopy (XAS) measurement, which comprises of both X-ray Near Edge Structure (XANES) and Extended X-ray Absorption Fine Structure (EXAFS) techniques, have been carried out on Cr doped YAGG at Cr, Ga and Y K-edges to probe the local structure. The XAS measurements have been carried out at the Energy-Scanning EXAFS beamline (BL-9) at the Indus-2 Synchrotron Source (2.5 GeV, 100 mA) at Raja Ramanna Centre for Advanced Technology (RRCAT), Indore, India.[1, 2] XAS measurements have been performed in fluorescence mode at Cr K-edge and in transmission mode at Ga and Y K-edge.

The absorption coefficient is obtained using the relation $\mu = I_f/I_0$. For the transmission measurement, three ionization chambers (300 mm length each) have been used for data collection, one ionization chamber for measuring incident flux (I_0), second one for measuring transmitted flux (I_t) and the third ionization chamber for measuring XAS spectrum of a reference metal foil for energy calibration. Appropriate gas pressure and gas mixtures have been chosen to achieve 10-20% absorption in first ionization chamber and 70-90% absorption in second ionization chamber to improve the signal to noise ratio. The absorption coefficient μ is obtained using the relation:

$$I_T = I_0 e^{-\mu x} \qquad \text{(S1)}$$

where, x is the thickness of the absorber. In case of fluorescence mode, silicon drift detector is used to measure the fluorescence intensity I_f and ionization chamber for measuring incident flux (I_0).

The oxidation state and coordination geometry corresponding to each element can be determined through the XANES spectroscopy. The absorption edge position with respect to known standards can give the oxidation states and different spectral features such as pre-edge could be useful to determine the coordination geometry of the absorbing element.

To simulate the theoretical EXAFS spectrum, structural parameters were obtained from a previously reported structure.[3] The XAS analysis was conducted using the Demeter package, incorporating ATHENA and ARTEMIS subroutines for data processing and analysis.[4] Fitting parameters, such as bond length and disorder factor (σ^2), were employed in the Y and Ga K-edge analysis. However, the Ga-O coordination have been derived from the contribution of two crystallographic sites with tetrahedral and octahedral coordination. In the context of Cr K-edge analysis, the coordination number was systematically varied. The fractional occupancy of distinct scattering paths between Ga and Al sites was carefully adjusted based on their respective theoretical values derived directly from theoretical coordination numbers. Similar scattering paths were amalgamated, each with its corresponding weights for Ga and Al scatterers.

S3. Computational Details

To model the defect containing $Y_3Al_2Ga_3O_{12}$, we have chosen 160□ atoms cell for $Y_3Al_2Ga_3O_{12}$ (Y:24, Al:16, Ga:24 O:96). The defect formation energies for different defect systems have been calculated using the mathematical relationship below.[5, 6]

$$E_{formation} = E_{defect} - E_{perfect} + q\sum n_x \mu_x \quad \text{(S2)}$$

where, E_{defect} and $E_{perfect}$ represent the energy of the doped and perfect $Y_3Al_2Ga_3O_{12}$, calculated with same cell size, μ_x indicate the chemical potential of the element X and n_x is the number of elements added (q=-1) or replaced (q =+1) to form the defect system. It can be noted that lower the defect formation energy higher the probability of the formation of the defect containing system.

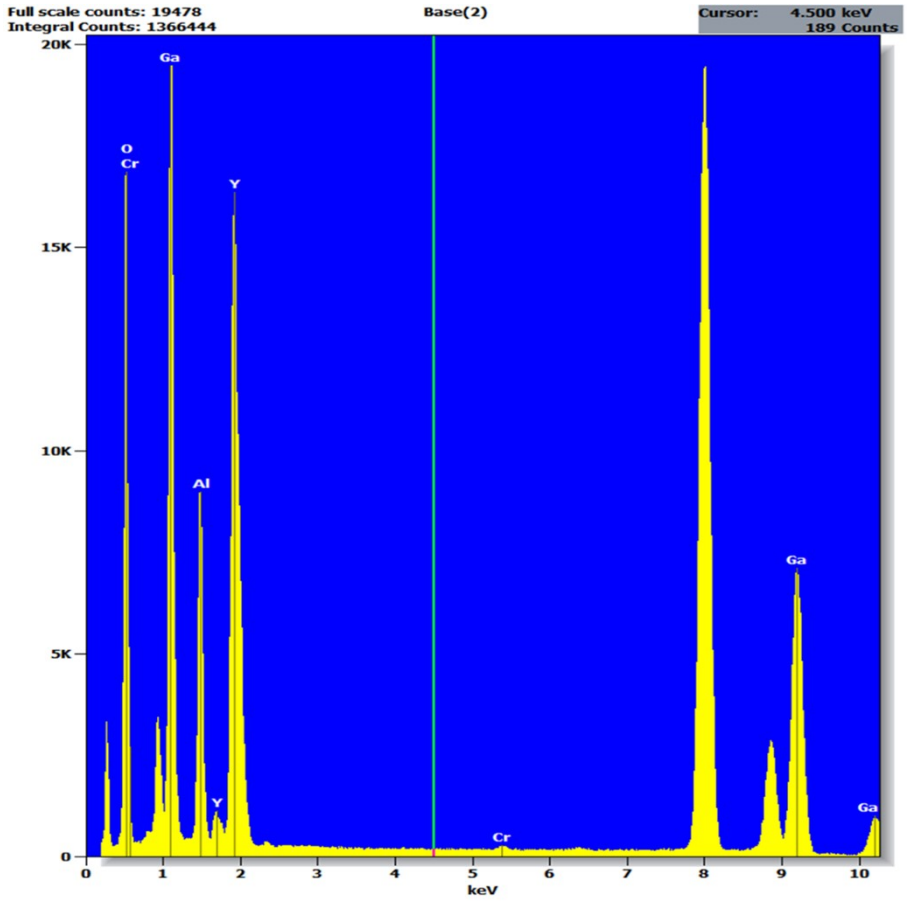

Figure S1: EDS spectrum of YAGG: 0.04Cr sample.

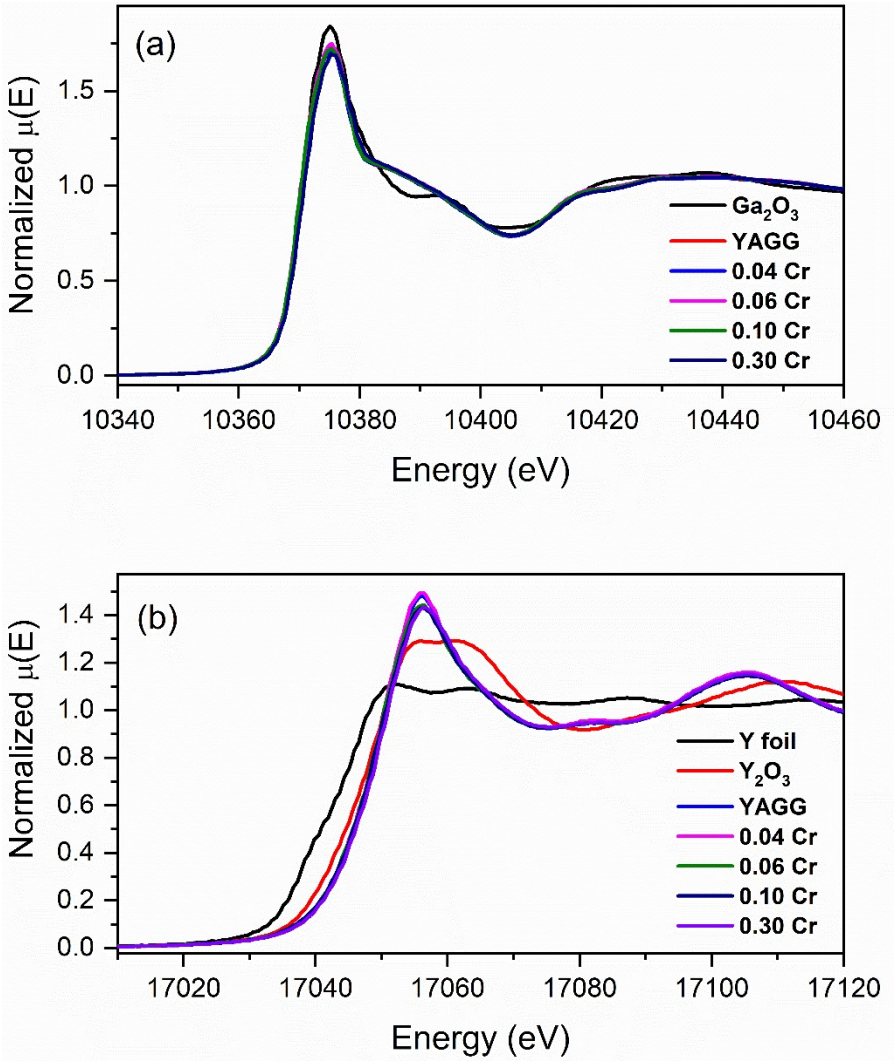

Figure S2: Normalised XANES spectra at (a) Ga K-edge and (b) Y K-edge along with that of their respective standards.

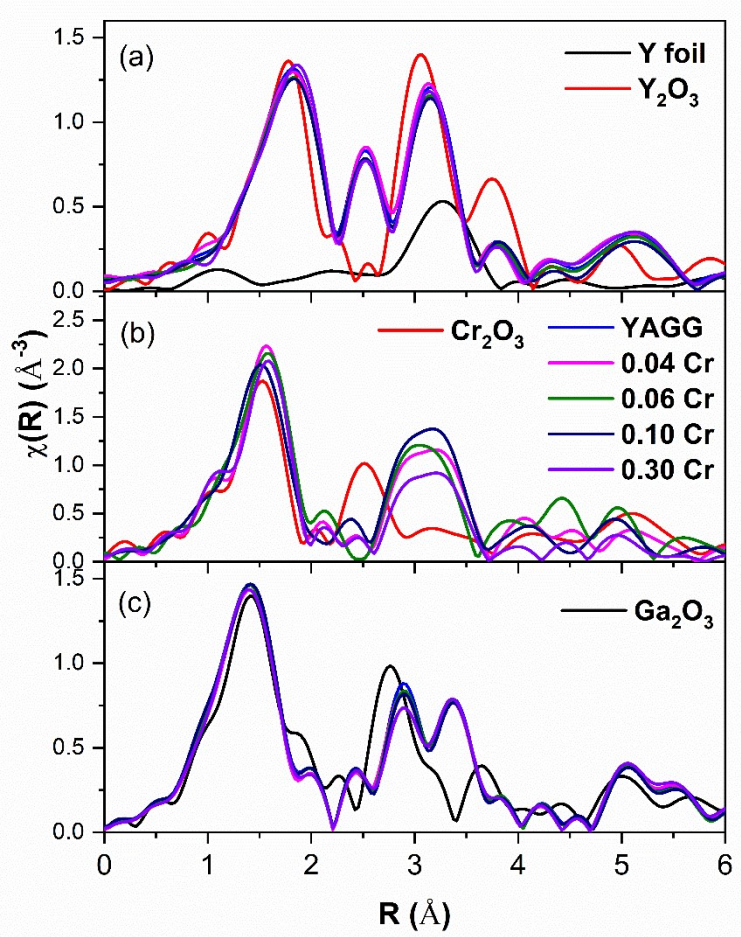

Figure S3: Fourier transformed EXAFS spectrum of undoped and Cr doped YAGG at (a) Y K-edge, (b) Cr K-edge and (c) Ga K-edge along with that of their respective standards.

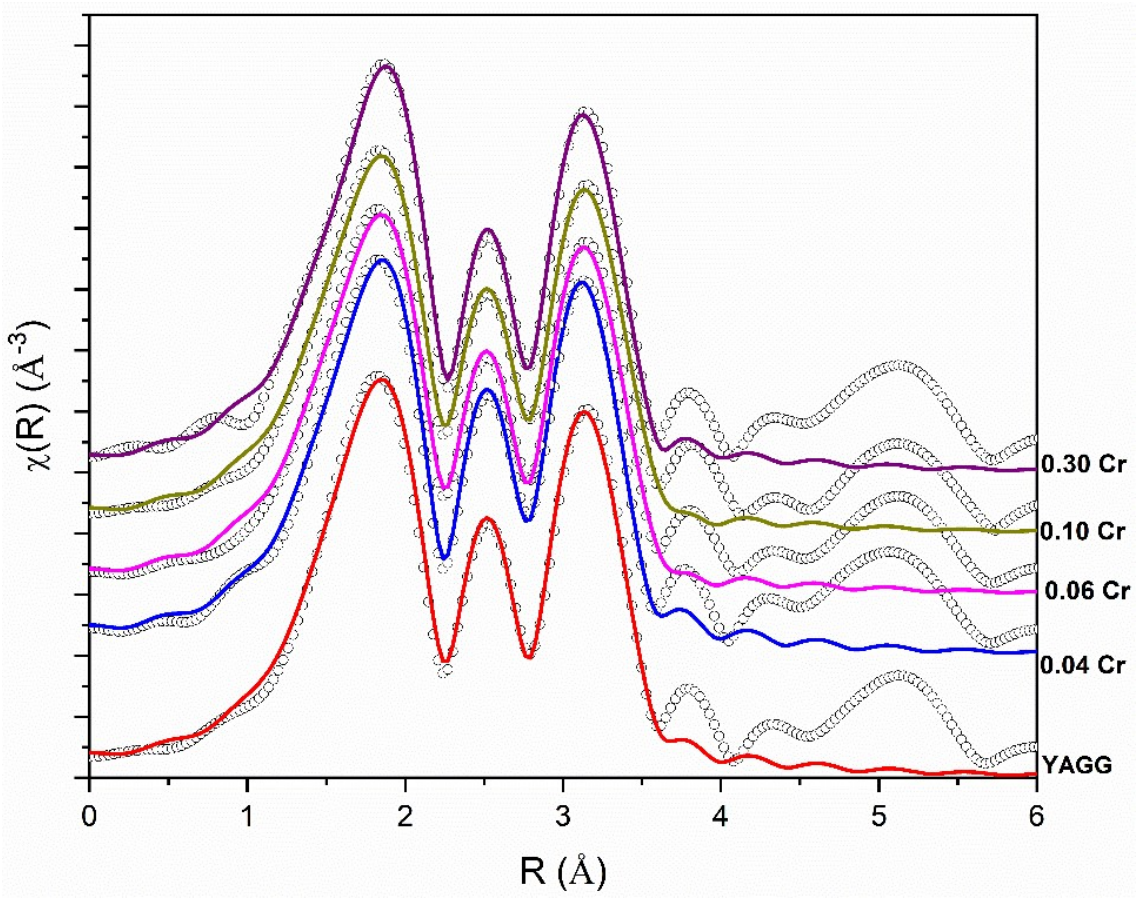

Figure S4: Fourier transformed EXAFS spectrum (scatter points) and their respective fittings (solid line) of undoped and Cr doped YAGG at Y K-edge. The spectra are vertically shifted for better illustration.

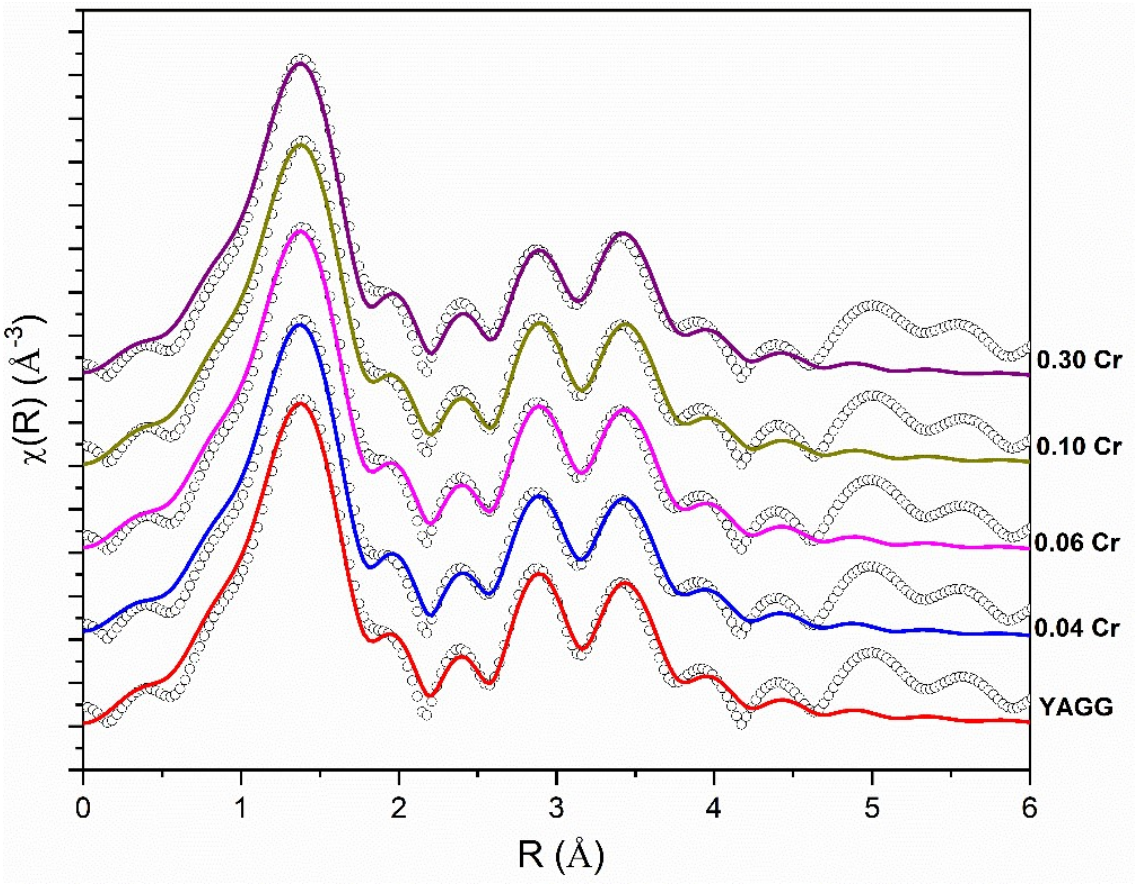

Figure S5: Fourier transformed EXAFS spectrum (scatter points) and their respective fittings (solid line) of undoped and Cr doped YAGG at Ga K-edge. The spectra are vertically shifted for better illustration.

Table S1: Bond length, coordination number and disorder factor obtain by EXAFS fitting at Y K-edge.

Path	Parameters	YAGG	YAGG:2% Cr	YAGG:3% Cr	YAGG:5% Cr	YAGG:15% Cr
Y-O	R (Å)	2.32±0.02	2.32±0.02	2.32±0.02	2.32±0.02	2.33±0.01
	N	4	4	4	4	4
	σ^2 (Å^2)	0.0046±0.0016	0.0045±0.0014	0.0052±0.0017	0.0053±0.0016	0.0047±0.0014
Y-O	R (Å)	2.45±0.02	2.46±0.02	2.45±0.03	2.45±0.03	2.46±0.03
	N	4	4	4	4	4
	σ^2 (Å^2)	0.0046±0017	0.0045±0015	0.0052±0018	0.0053±0016	0.0047±0014
Y-Ga/Al	R (Å)	3.07±0.03	3.08±0.02	3.08±0.01	3.08±0.01	3.10±0.02
	N	4	4	4	4	4
	σ^2 (Å^2)	0.0037±0.0029	0.0028±0.0023	0.0046±0.0035	0.0045±0.0031	0.0028±0.0021
Y-Al/Ga	R (Å)	3.43±0.03	3.43±0.01	3.43±0.03	3.42±0.03	3.40±0.02
	N	8	8	8	8	8
	σ^2 (Å^2)	0.0020±0.0015	0.0021±0.0019	0.0020±0.0011	0.0022±0.0018	0.0021±0.0015
Y-Ga/Al	R (Å)	3.85±0.02	3.87±0.03	3.87±0.02	3.82±0.02	3.88±0.02
	N	8	8	8	8	8
	σ^2 (Å^2)	0.0181±0.0056	0.0196±0.0038	0.0147±0.0061	0.0142±0.0064	0.0192±0.0038

Table S2: Bond length, coordination number and disorder factor obtain by EXAFS fitting at Ga K-edge.

Path	Parameters	YAGG	YAGG: 2% Cr	YAGG: 3% Cr	YAGG: 5% Cr	YAGG: 15% Cr
Ga-O	**R (Å)**	1.85±0.01	1.84±0.01	1.85±0.01	1.85±0.01	1.84±0.01
	N	5.17±0.32	4.71±0.43	5.06±0.38	5.06±0.55	4.65±0.63
	σ^2 (Å^2)	0.0102±0.0020	0.0089±0.0021	0.0098±0.0019	0.0100±0.0019	0.0089±0.0019
Ga-Y	**R (Å)**	3.43±0.01	3.43±0.01	3.43±0.01	3.43±0.02	3.44±0.01
	N	6	6	6	6	6
	σ^2 (Å^2)	0.0064±0015	0.0061±0016	0.0067±0015	0.0070±0016	0.0072±0017
Ga-Al/Ga	**R (Å)**	3.43±0.03	3.43±0.02	3.43±0.01	3.43±0.01	3.44±0.01
	N	6	6	6	6	6
	σ^2 (Å^2)	0.0064±0.0015	0.0063±0.0016	0.0067±0.0015	0.0070±0.0016	0.0072±0.0017
Ga-Y	**R (Å)**	3.66±0.03	3.66±0.02	3.66±0.02	3.67±0.01	3.67±0.01
	N	6	6	6	6	6
	σ^2 (Å^2)	0.0041±0.0014	0.0035±0.0013	0.0040±0.0012	0.0041±0.0013	0.0032±0.0012
Ga-Ga/Al	**R (Å)**	3.66±0.02	3.66±0.02	3.66±0.01	3.67±0.01	3.67±0.01
	N	4	4	4	4	4
	σ^2 (Å^2)	0.0041±0.0014	0.0035±0.0013	0.0040±0.0012	0.0041±0.0013	0.0032±0.0012

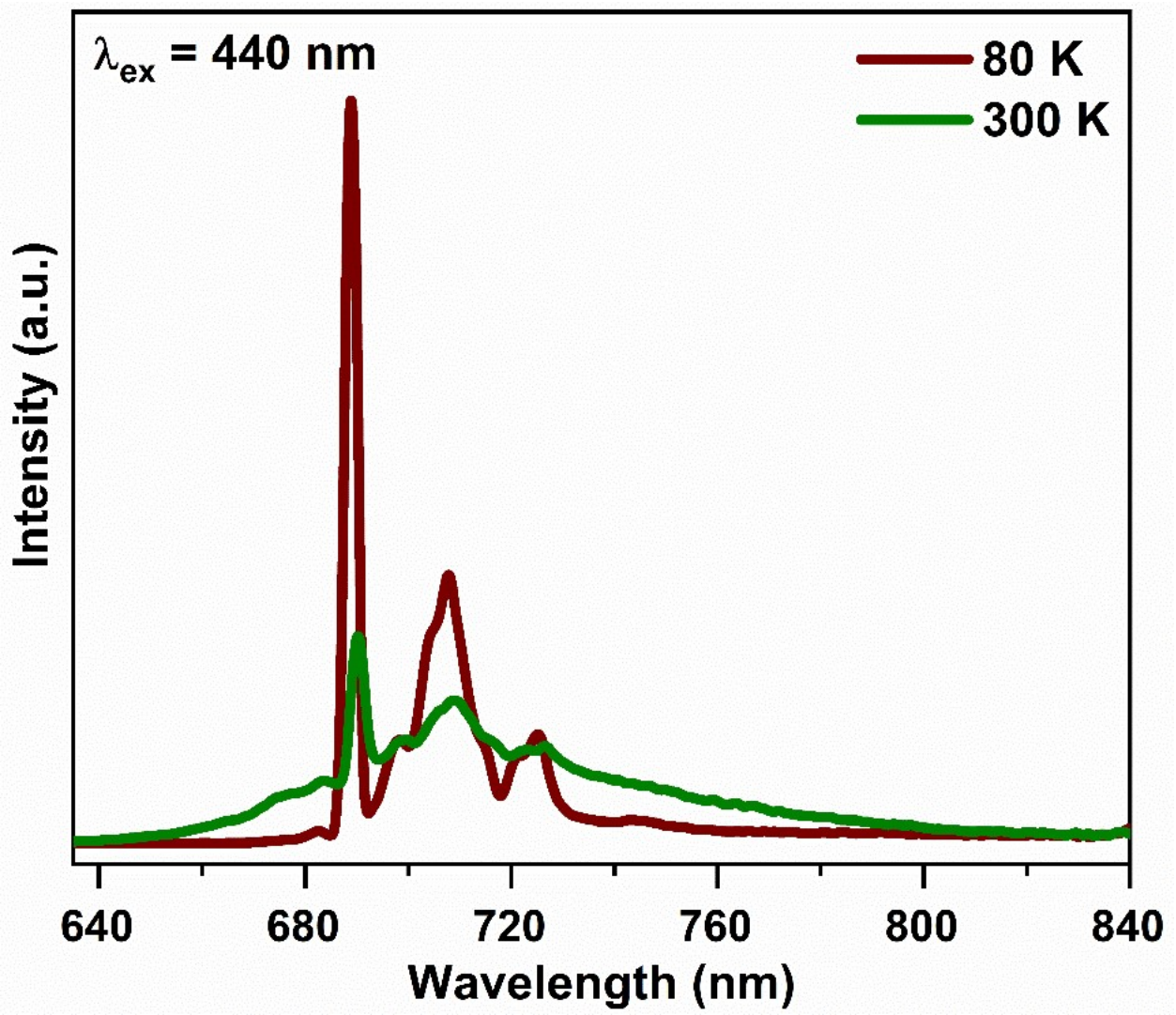

Figure S6: PL emission spectra of YAGG:0.04Cr phosphor at 80 and 300 K.

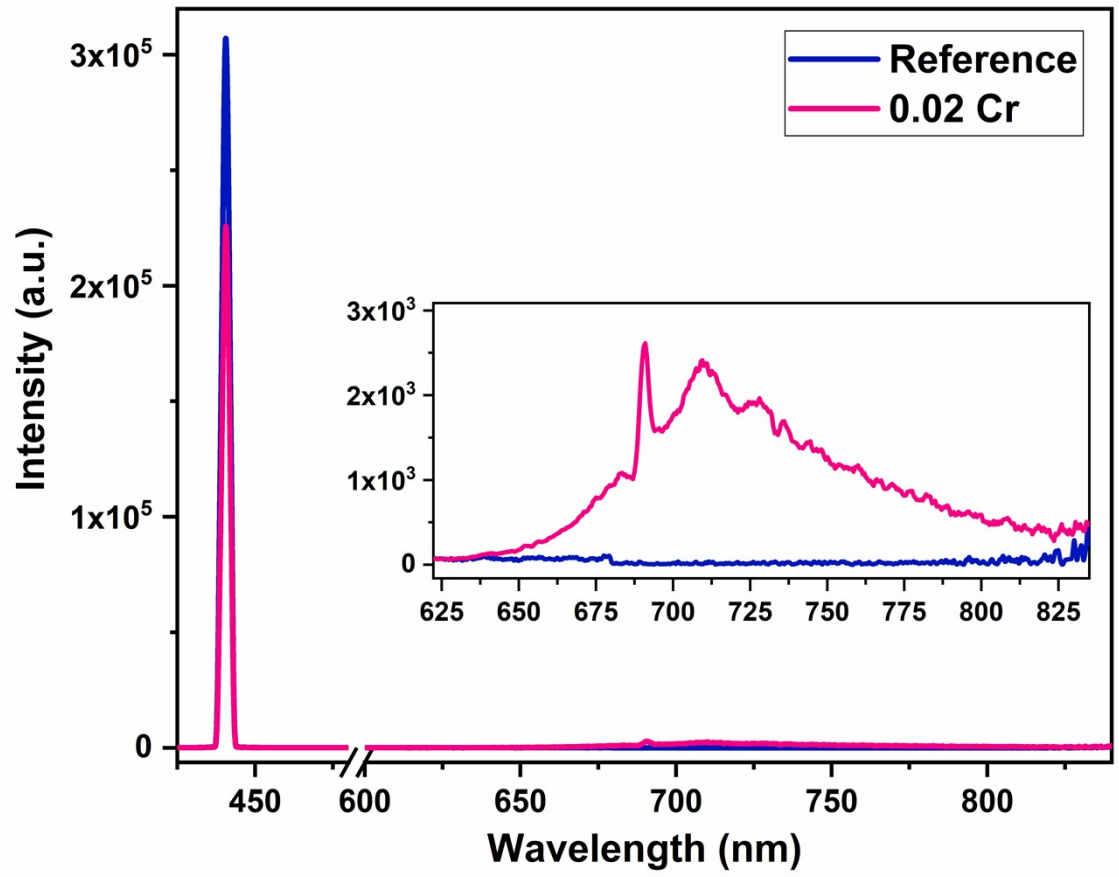

Figure S7: Scattering peaks and emission spectra for quantum yield measurement of YAGG:0.04Cr phosphor with respect to reference.

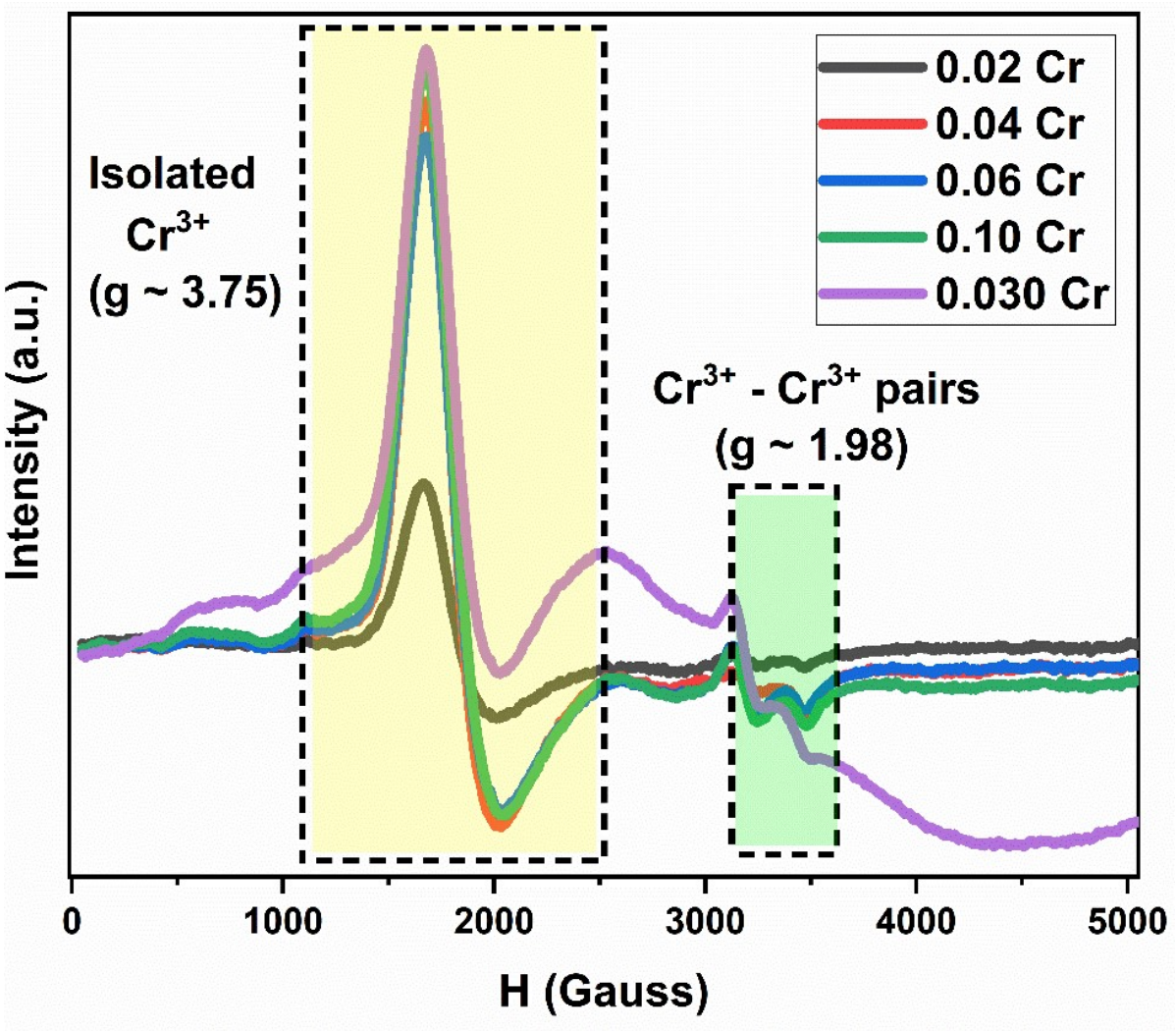

Figure S8: EPR spectra of Cr^{3+}-doped YAGG phosphors at 100 K.

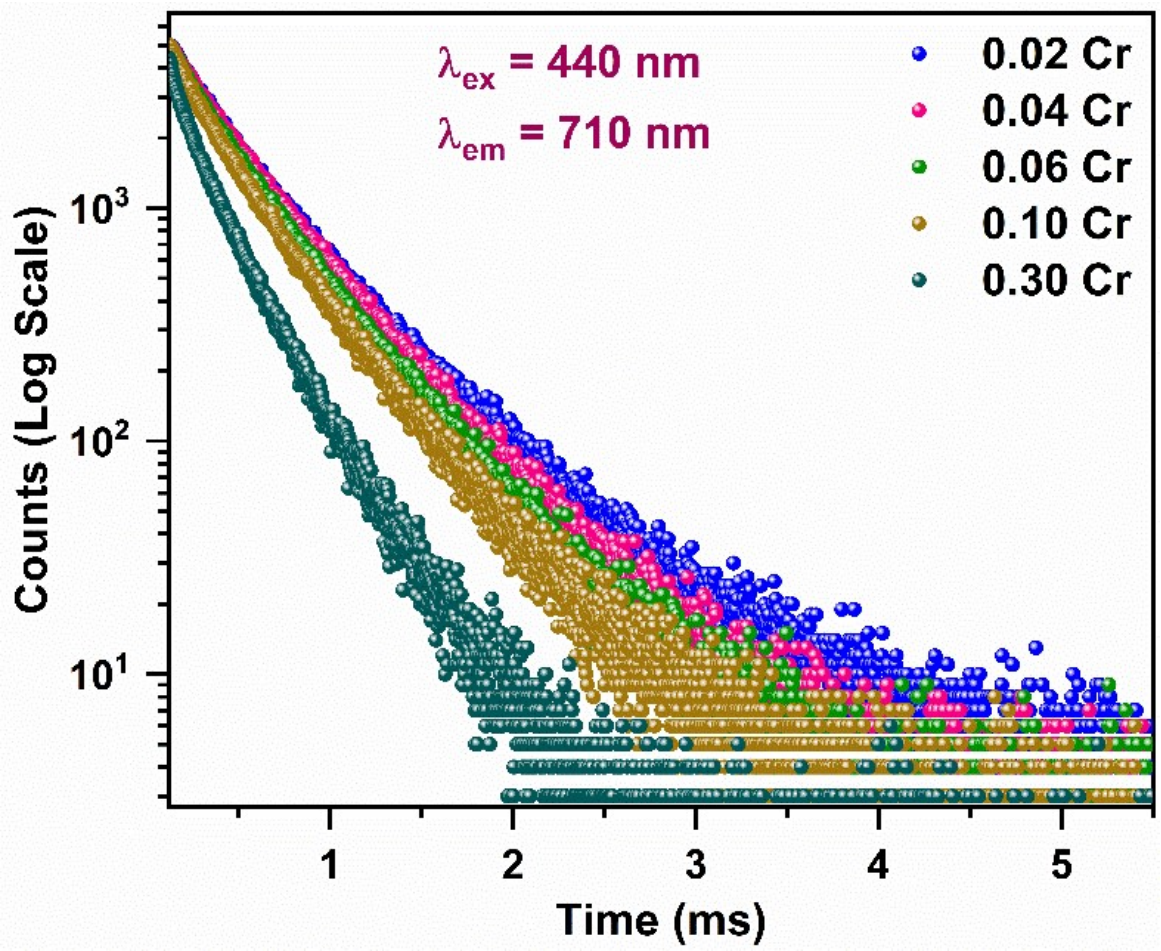

Figure S9: Decay curves monitored at 710 nm of YAGG: xCr^{3+} (x = 0.02–0.30 mol) upon 440 nm excitation.

Table S3: Lifetime values of Cr^{3+}-doped YAGG phosphors under 440 nm excitation, and monitoring emissions at 690, 710, and 750 nm.

λ_{ex} = 440 nm and λ_{em} = 690 nm					
	τ_1 (μs)	%	τ_2 (μs)	%	τ_{avg} (μs)
0.02 Cr	300.2	45.7	626.7	54.3	477.6
0.04 Cr	283.6	37.6	532.1	65.4	454.7
0.06 Cr	234.2	30.6	484.1	69.4	407.6
0.1 Cr	220.1	34.9	468.6	65.1	381.8
0.3 Cr	119.5	26.1	314.3	73.9	263.5
λ_{ex} = 440 nm and λ_{em} = 710 nm					
	τ_1 (μs)	%	τ_2 (μs)	%	τ_{avg} (μs)
0.02 Cr	293.9	46.8	638.4	53.2	477.1
0.04 Cr	272.8	34.8	530.2	65.2	440.5
0.06 Cr	229.9	31.4	486.3	68.6	405.7
0.1 Cr	213.9	35.4	465.3	64.6	376.3
0.3 Cr	136.8	28.8	322.0	71.2	268.6
λ_{ex} = 440 nm and λ_{em} = 750 nm					
	τ_1 (μs)	%	τ_2 (μs)	%	τ_{avg} (μs)
0.02 Cr	240.2	38.7	574.6	61.4	445.4
0.04 Cr	239.9	29.7	508.0	70.3	428.4
0.06 Cr	198.4	28.7	464.6	71.3	388.1
0.1 Cr	206.4	39.7	459.4	60.4	359.1
0.3 Cr	124.8	30.1	315.0	69.9	257.8

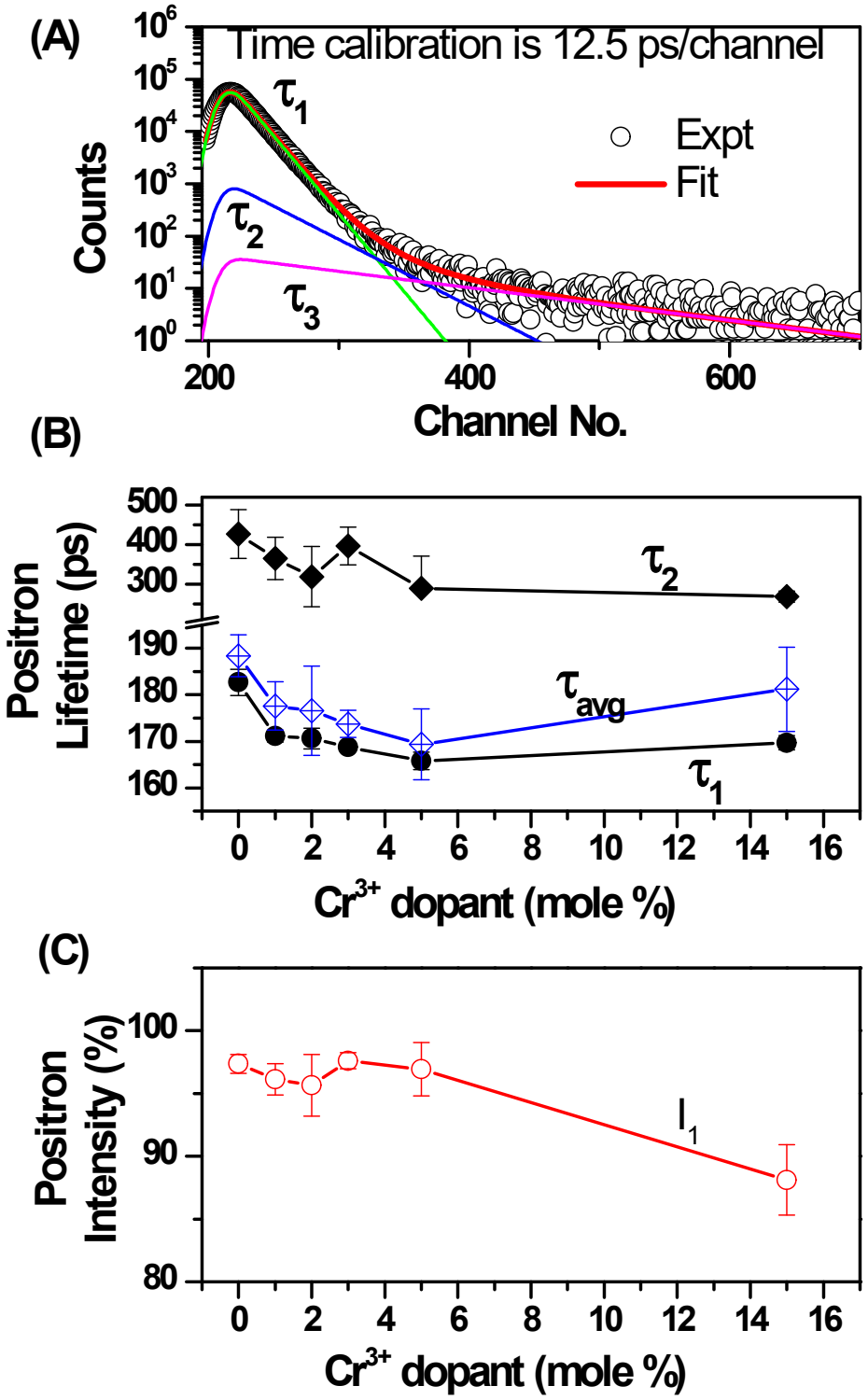

Figure S10: (a) Typical fitting of the positron annihilation lifetime spectrum to extract lifetimes, (b) individual positron lifetimes and the intensity weighted average positron lifetimes in Cr^{3+} doped YAG samples, and (c) fraction intensity of positrons annihilating from bulk positron states corresponding to τ_1.

Table S4: Calculated defect formation energies for different types of defects in $Y_3Al_2Ga_3O_{12}$.

System	Defect Formation Energy (eV)
Y-vacancy (V_Y)	13.40
Al-vacancy (V_{Al})	12.72
Ga-vacancy (V_{Ga})	8.53
O-vacancy (V_O)	4.62
Ga-Al-vacancy (V_{Ga}, V_{Al})	21.25
Y-O-vacancy (V_Y, V_O)	13.89
Al-O-vacancy (V_{Al}, V_O)	12.76
Ga-O-vacancy (V_{Ga}, V_O)	7.96

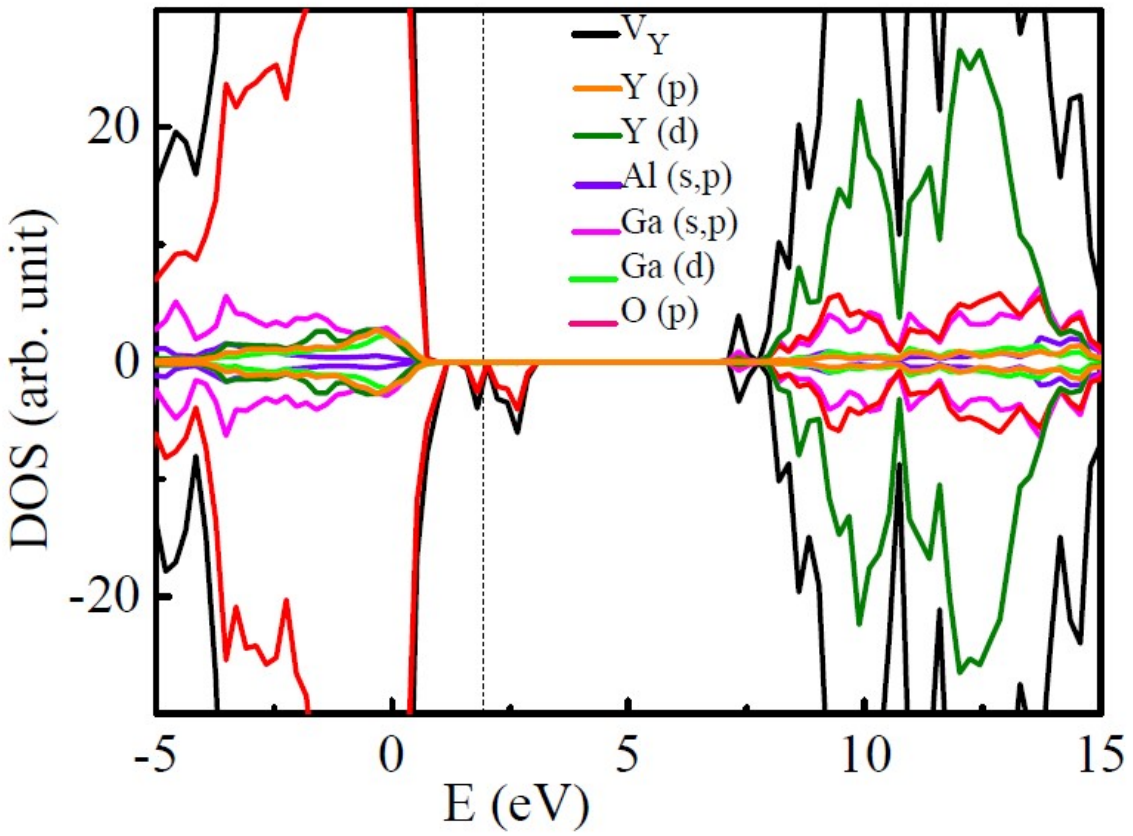

Figure S11: Density of states of $Y_3Al_2Ga_3O_{12}$ in the presence of one neutral yttrium vacancy. Vertical dashed line indicates the Fermi level.

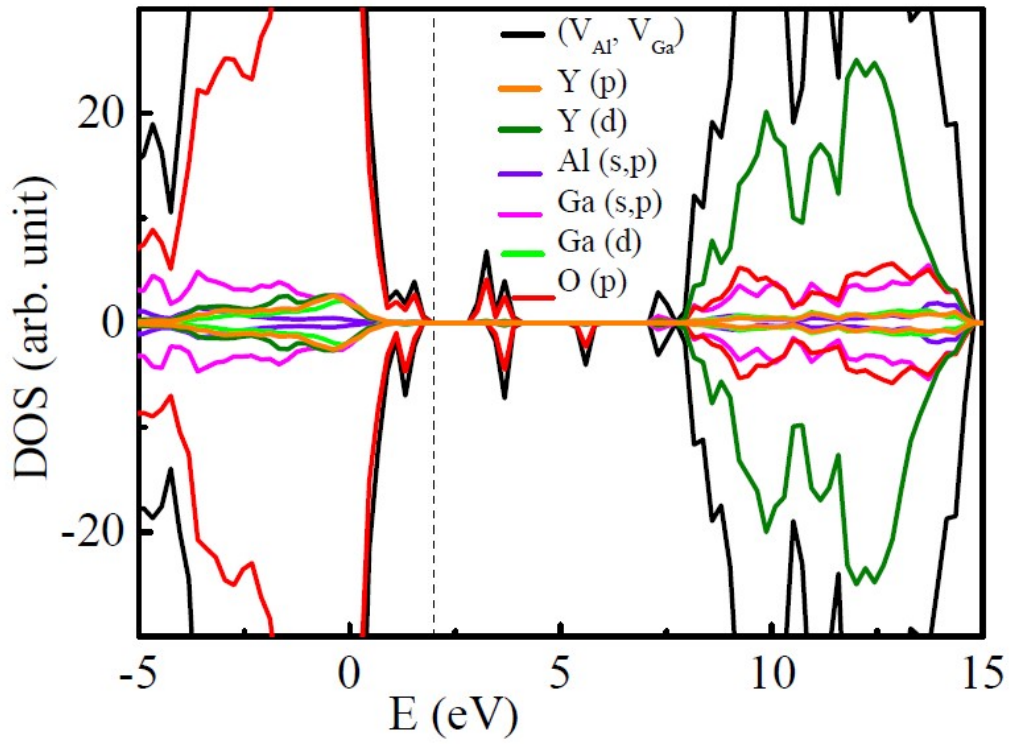

Figure S12: (a) DOS of $Y_3Al_2Ga_3O_{12}$ in the presence of one neutral aluminium and gallium vacancy. Vertical dashed line indicates the Fermi level.

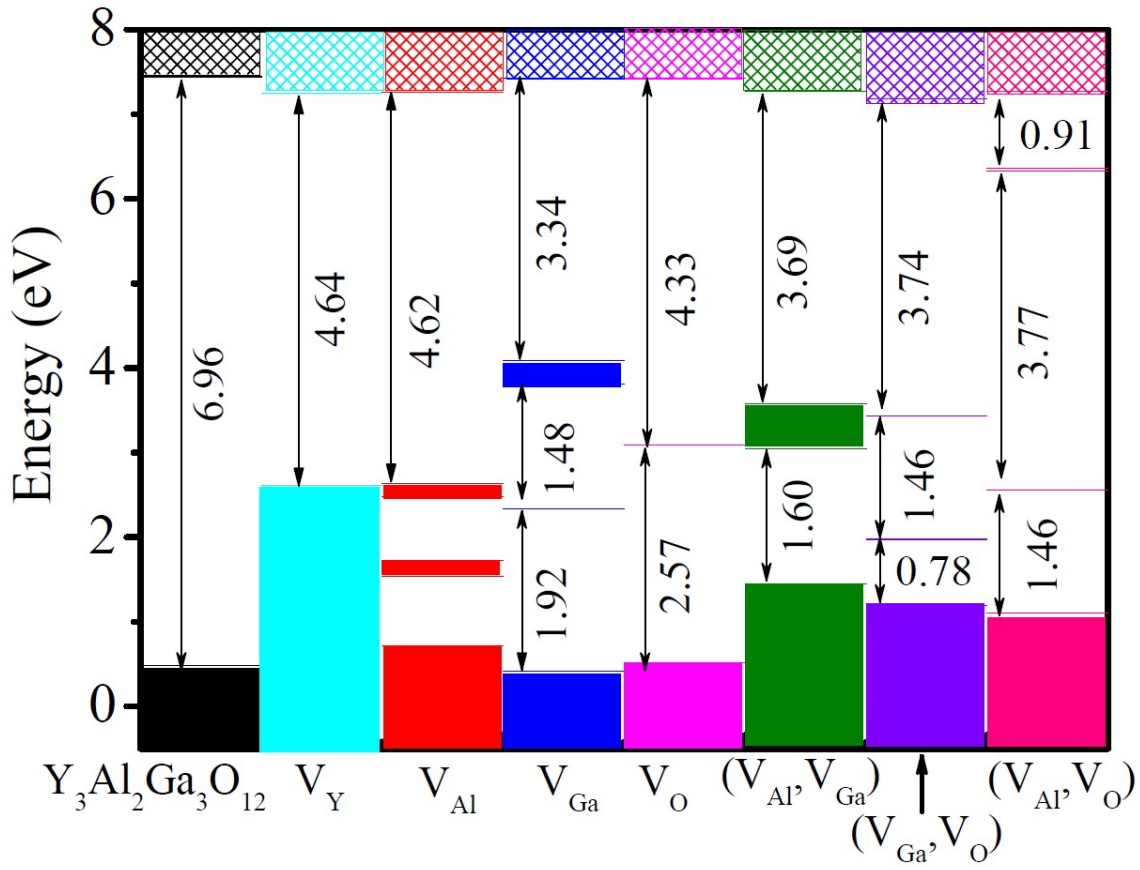

Figure S13: Relative positions of band edges and impurity levels for the defect containing $Y_3Al_2Ga_3O_{12}$.

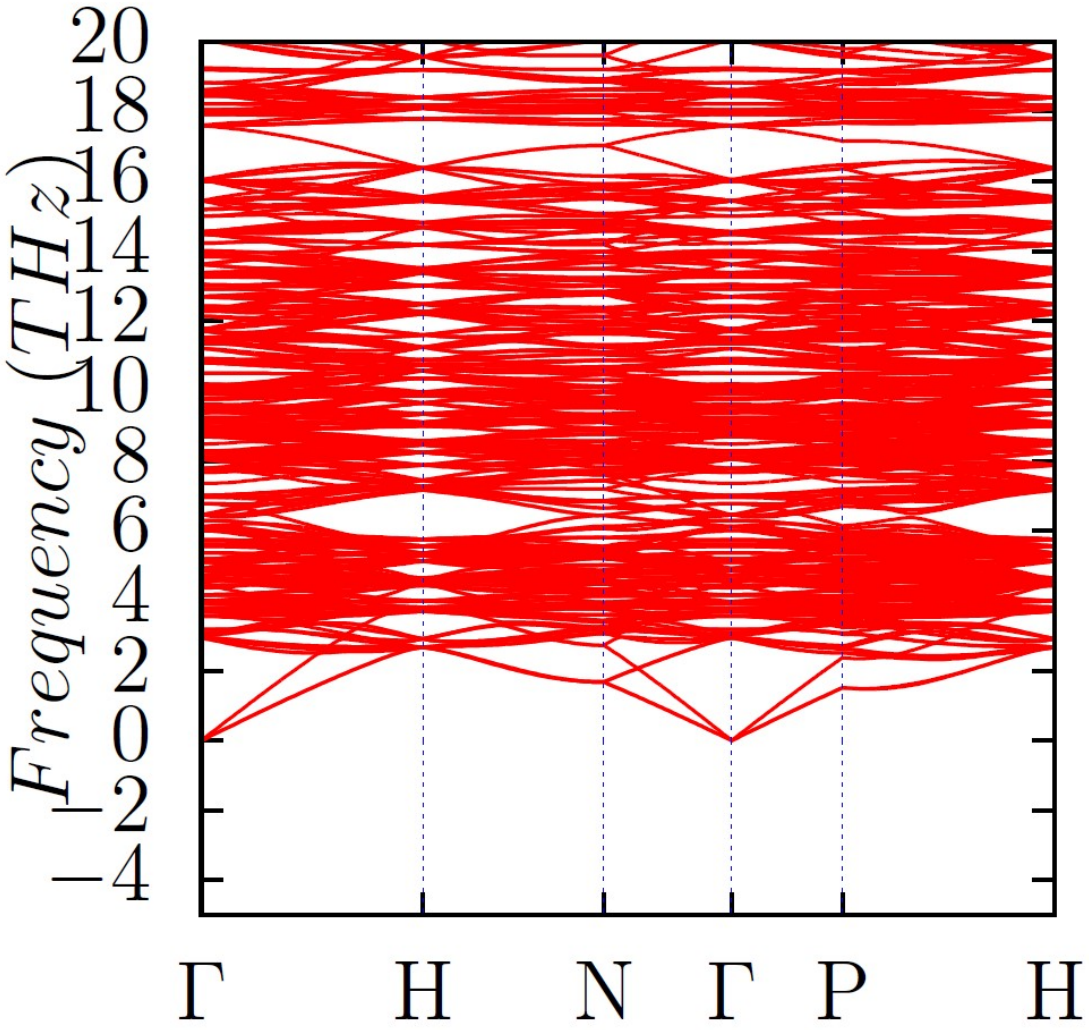

Figure S14: Phonon dispersion plot of $Y_3Al_2Ga_3O_{12}$.

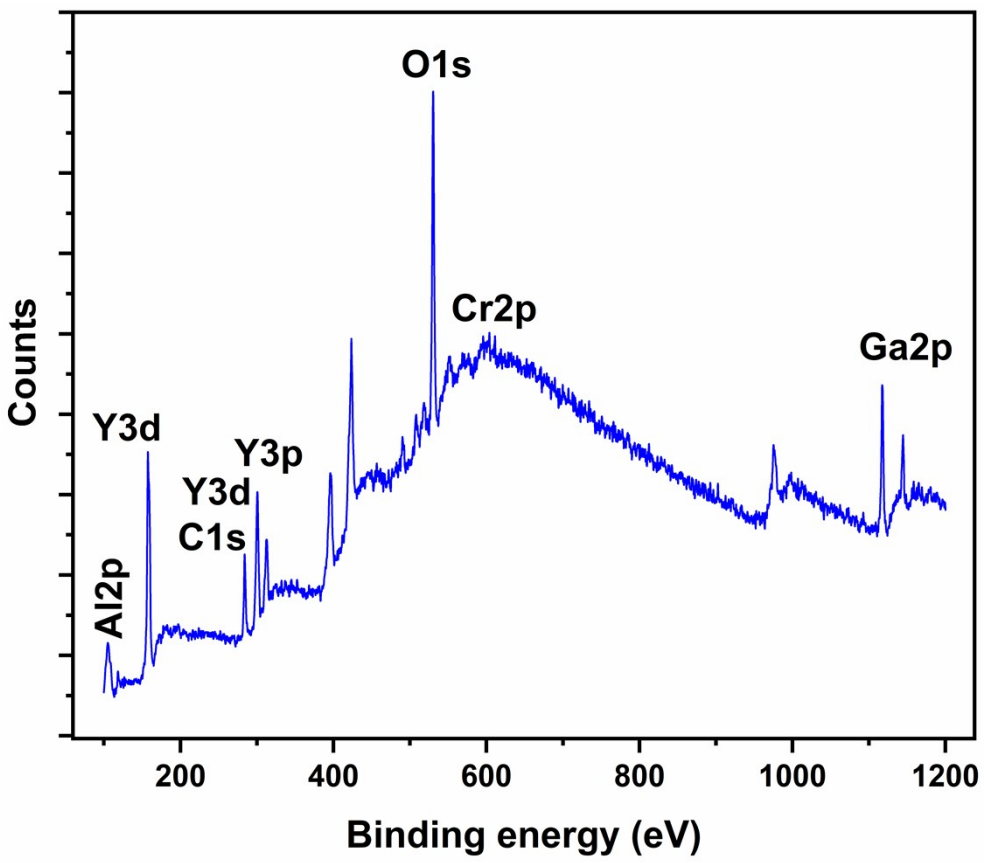

Figure S15: XPS spectrum of YAGG:0.04Cr^{3+} sample.

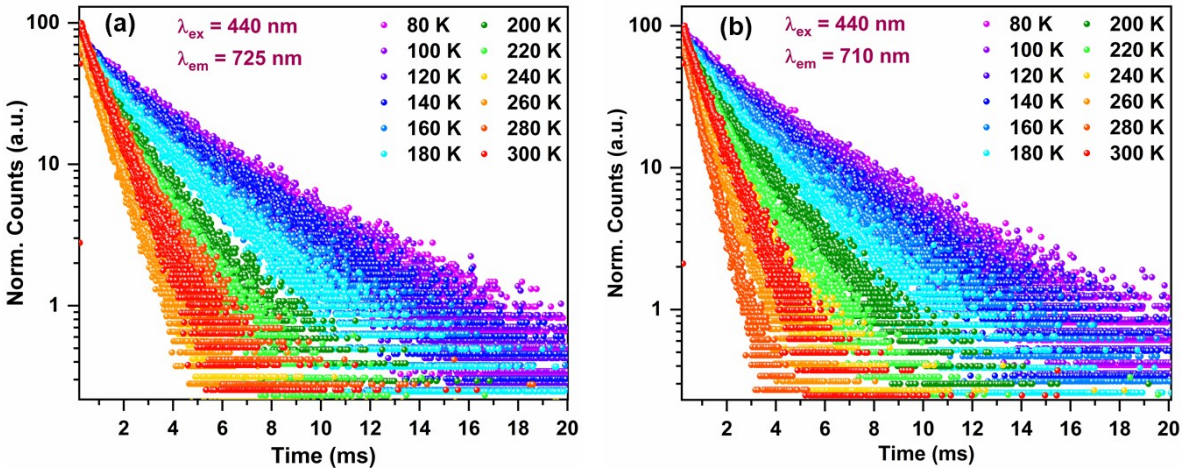

Figure S16: Decay curves of YAGG: $x$$Cr^{3+}$ (x = 0.02–0.30 mol) upon 440 nm excitation and monitored at (a) 725 and (b) 710 nm.

Table S5: Decay lifetimes of YAGG: xCr^{3+} (x = 0.02–0.30 mol) upon 440 nm excitation and monitoring at 690, 710, and 725 nm, respectively.

T (K)	λ_{em} = 690 nm (ms)	λ_{em} = 710 nm (ms)	λ_{em} = 725 nm (ms)
80	3.314	3.279	3.258
100	3.353	3.28	3.248
120	3.196	3.129	3.068
140	2.821	2.887	2.963
160	2.624	2.536	2.456
180	1.982	2.153	2.233
200	1.8067	1.731	1.637
220	1.342	1.362	1.431
240	1.079	1.019	0.9323
260	0.7539	0.7929	0.8364
280	0.6539	0.5912	0.5504
300	0.4599	0.4734	0.489

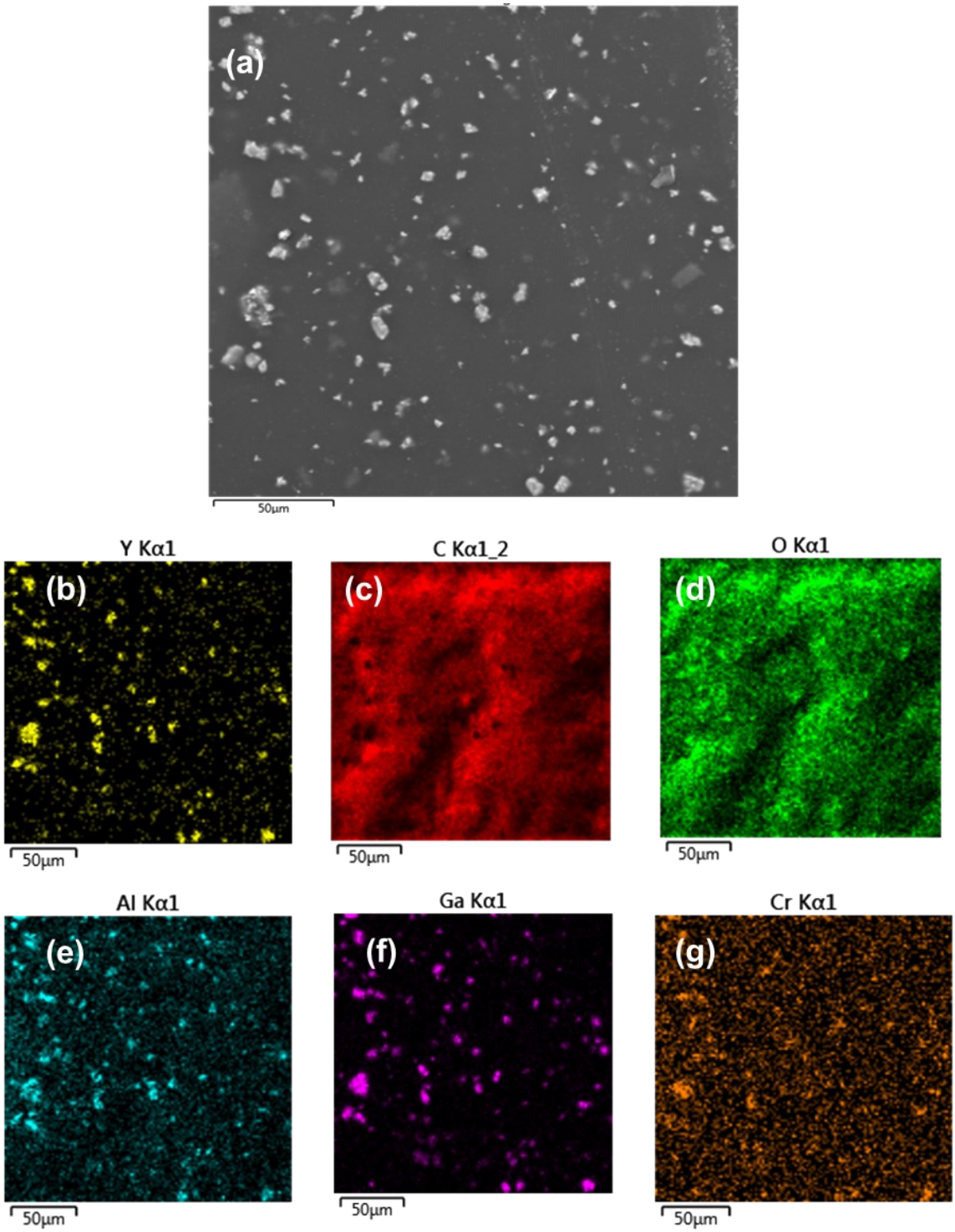

Figure S17: (a) Electron image of YAGG:0.04Cr^{3+} thin film, (b-g) Elemental mapping of Y, C, O, Al, Ga, and Cr elements in fabricated YAGG:0.04Cr^{3+} thin film, respectively.

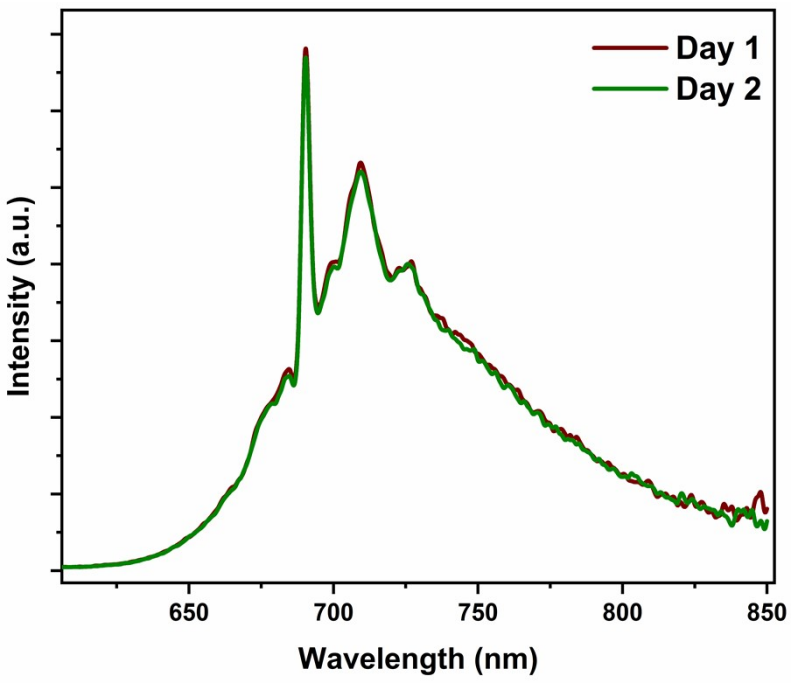

Figure S18: PL emission spectra of YAGG:0.04Cr^{3+} thin film after one day in water.

References:

1. Basu, S.; Nayak, C.; Yadav, A.; Agrawal, A.; Poswal, A.; Bhattacharyya, D.; Jha, S.; Sahoo, N. In *A comprehensive facility for EXAFS measurements at the INDUS-2 synchrotron source at RRCAT, Indore, India*, Journal of Physics: Conference Series, 2014; IOP Publishing: 2014; p 012032.

2. Poswal, A.; Agrawal, A.; Yadav, A.; Nayak, C.; Basu, S.; Kane, S.; Garg, C.; Bhattachryya, D.; Jha, S.; Sahoo, N. In *Commissioning and first results of scanning type EXAFS beamline (BL-09) at INDUS-2 synchrotron source*, AIP Conference Proceedings, 2014; American Institute of Physics: 2014; pp 649-651.

3. Nakatsuka, A.; Yoshiasa, A.; Yamanaka, T., Cation distribution and crystal chemistry of $Y_3Al_{5-x}Ga_xO_{12}$ ($0 \leq x \leq 5$) garnet solid solutions. *Acta Crystallographica Section B: Structural Science* **1999,** 55, (3), 266-272.

4. Ravel, B.; Newville, M., ATHENA, ARTEMIS, HEPHAESTUS: data analysis for X-ray absorption spectroscopy using IFEFFIT. *Journal of synchrotron radiation* **2005,** 12, (4), 537-541.

5. Modak, P.; Modak, B., Exploring the role of vacancy defects in the optical properties of $LiMgPO_4$. *Physical Chemistry Chemical Physics* **2020,** 22, (28), 16244-16257.

6. Modak, P.; Modak, B., Electronic structure investigation of intrinsic and extrinsic defects in LiF. *Computational Materials Science* **2022,** 202, 110977.